An experimental study on element migration and pore evolution during supercritical carbon dioxide geological sequestration in deep coal seams of the Ningxia region, China

Jie Xu[1], Yu Ma[2,3*], Beiqu Cui[2,3], Lirong Ma[2,3], Jingxiong Tian[2,3], Wenzhong Wu[2,3], Yong Zhang[2,3], Shangjie Hou[2,3]，Shengjin Huang[2,3]，Lili Wang[2,3]

[1] Bailie School of Petroleum Engineering, Lanzhou City University, Lanzhou, Gansu 730000, China

[2] Ningxia Institute of Basic Geological Survey, Yinchuan 750000, China

[3] Ningxia Key Laboratory of Geological Resources Exploration and Green Exploitation

* Corresponding author
E-mail: mayugeology@163.com (YM)

Abstract： With the intensification of global climate change, reducing greenhouse gas emissions has become a global challenge. As a high-emission region, Ningxia faces significant pressure to reduce emissions. Geological storage of carbon dioxide is considered one of the key technologies for achieving carbon neutrality. Utilizing deep unmineable coal seams for CO_2 sequestration can not only reduce greenhouse gas emissions but also increase the recovery rate of coalbed methane. However, the microscale interaction mechanisms between supercritical CO_2($scCO_2$) and coal seams in this region are not yet fully understood. Therefore, this study selected the No. 6 coal seam of the Jurassic Yan'an Formation in Ningxia as the research object and conducted $scCO_2$-water-coal simulation experiments using a high-temperature and high-pressure thermosimulation reactor. The experiments were set at 40℃ and 9MPa to simulate a geological environment at a depth of 1000 meters. The simulation experiments were divided into four groups with durations of 1, 3, 5, and 7 days. Laser ablation inductively coupled plasma mass spectrometry (LA-ICP-MS) and inductively coupled plasma optical emission spectrometry (ICP-OES) were used to analyze the elemental migration characteristics of the reaction solution and solid samples. Low-temperature N_2 and CO_2 gas adsorption methods were employed to study the evolution characteristics of pore structures. The experimental results showed that the main elements in the reaction solution were Ca, Na, and Mg. Additionally, 14 trace elements were detected, with concentrations being relatively low. Among them, Cr, Pb, Cu, Zn, and Ti were detected in the reaction solution, but their concentrations were all below 3 ppm. Analysis of elemental migration rates indicated that Mo, Nb, V, Cu, Rb, Pb, and Zn had high migration rates (average migration rates > ±50%), while Be, Co, and Y had migration rates below 10%. Low-temperature gas

adsorption experiments revealed that after $scCO_2$ treatment, the micropores in coal samples significantly increased, mesopores (1-50 nm) decreased, and macropores (>50 nm) slightly increased. This suggests that the microporous structure of coal seams was enhanced after $scCO_2$ treatment, which is conducive to the adsorption and sequestration of CO_2. Moreover, the release of potentially harmful elements was extremely low, indicating high safety for this region as a CO_2 sequestration site. This research provides important scientific evidence and technical support for CO_2 geological storage in Ningxia and even nationwide.

Keyword: $ScCO_2$-H_2O-coal; Low-rank coal; Pore structure; Element change; Ningxia region

1.Introduction

Climate change, driven by rising global temperatures due to greenhouse gas emissions, is a critical environmental challenge. The Intergovernmental Panel on Climate Change (IPCC) reported a 1.1℃ increase in global temperatures, primarily attributed to CO_2 emissions from fossil fuel use[1]. Achieving carbon neutrality is a global imperative. China has pledged to peak CO_2 emissions before 2030 and achieve carbon neutrality by 2060[2]， which is a formidable challenge for high-emission regions such as Ningxia.

Carbon Capture, Utilization, and Storage (CCUS) is a key strategy to mitigate CO_2 emissions. And the carbon storage is the last but most important step of the strategy. Suitable sites for geological CO_2 sequestration need to meet the following characteristics: (1) the reservoir rocks must have sufficient porosity and permeability to accommodate and transport large amounts of CO_2[3,4]; (2) at the same time, the caprock above the reservoir must be impermeable to prevent CO_2 from leaking to the surface or shallow aquifers[5,6]; (3) in addition, the reservoir area should have stable geological structures with few faults and fractures to minimize the risk of leakage[7,8]. Of course, when selecting a site, it is also necessary to consider the potential impact on groundwater resources and the ecological environment to ensure the safety and sustainability of the sequestration process[9]. The mainly targets geological formation for carbon storage include depleted oil and gas reservoirs, deep saline aquifers, unminable deep coal seams, and so on[10]. Among these options, the potential of utilizing unmineable coal seams for CO_2 storage was first recognized in the early 2000s[11]. Since then, it has been regarded as one of the most promising approaches for CO_2 geological sequestration under certain specific conditions. Because it not only sequesters carbon dioxide in unmineable coal seams but also increases the production of coalbed methane[12,13,14]. Meanwhile, Coal seams possess a significantly higher adsorption affinity for CO_2 compared to CH_4, which represents a critical advantage for CO_2 geological storage.

Previous studies have demonstrated that the CO_2 adsorption capacity of coal matrix is more than twice that of CH_4 on a molar basis[11]. This preferential adsorption behavior enables CO_2 to be securely stored in coal seams in an adsorbed state over extended periods, thereby effectively mitigating the risk of CO_2 leakage into the atmosphere[15,16].

So far, many international and domestic pilot projects have proved the feasibility of storing carbon dioxide in deep coal seams. For instance, the United States injected over 10^5 tons of CO_2 into coal seams in the San Juan Basin, and the European Union's RECOPOL project has successfully conducted CO_2 injection into the coal seams of the Silesian Basin in Poland, with a total volume of 760 tons[17,18].Deep coal seams are extensively developed in China. Liu et al. (2005) and Li et al. (2009) estimated using different methods that the geological storage capacity of CO_2 in China's coal seams is approximately 120×10^8 t[19,20]. From 2002 to 2006, a total of 192.8 tons of liquid CO_2 was injected into the No. 3 coal seam of the Shanxi Formation in the southern part of the Qinshui Basin in Shanxi, China. The results indicated that the storage performance was satisfactory[21].

Nevertheless, there are still many issues of concern when carbon dioxide is injected into deep underground coal seams. For instance, when the burial depth of targeted coal seams is >800 m, carbon dioxide becomes supercritical upon injection where the temperature and pressure reach 304.15 K and 7.38 MPa[22,23,24], respectively. Supercritical fluids represent a unique state that lies between gases and liquids, exhibiting distinctive physical and chemical properties. Their primary characteristics include high density, high diffusivity, high solubility, low viscosity, and the absence of surface tension[25,26,27]. The density of supercritical fluids is significantly higher than that of gases and approaches that of liquids, thereby markedly enhancing their solvent capabilities and enabling effective dissolution of hydrophobic substances. Moreover, the diffusion coefficients of supercritical fluids are much higher than those of liquids and are comparable to those of gases, allowing for rapid penetration and transport of substances. Additionally, due to their high density and low viscosity, supercritical fluids possess strong solubility, capable of dissolving a wide range of organic and inorganic compounds. Their viscosity is similar to that of gases and much lower than that of liquids, which helps reduce mass transfer resistance and improve separation efficiency. Finally, the absence of surface tension in supercritical fluids means that they can mix uniformly with substances without forming interfaces, making certain chemical reactions and extraction processes more favorable. CO_2 is an intrinsically non-polar molecule[28]. Compared with other supercritical fluids, supercritical CO_2 ($scCO_2$) exhibits relatively weak polarity. Under normal conditions, it possesses good chemical stability and is unlikely to undergo chemical reactions with highly polar substances, resulting in relatively poor solubility[29,30,31]. However, it can dissolve some non-polar or low-polarity organic compounds, and the extent of its solubility capacity is related to the temperature and pressure conditions[32]. Meanwhile,

during the geological storage of carbon dioxide, when it is injected to a certain depth and transitions into a supercritical fluid, it will react with the water in the coal seam to form an weakly acidic fluid[33]. Owing to its unique physicochemical properties, this fluid will interact with the coal rock, resulting in structural alterations of the coal seams and the leaching release of harmful trace elements. In this process, the pore structure of the coal seams will be altered[34], which has a significant impact on the storage capacity and stability of carbon dioxide. Moreover, if the solution containing harmful trace elements migrates into the shallow aquifer, it will have a profound impact on groundwater quality. Consequently, when evaluating the feasibility of geological storage of CO_2 in deep coal seams, it is essential to investigate the potential modification effects of CO_2 on the coal seams.

Affected by economic development and the local resource structure, the total carbon emissions in the Ningxia region have shown a continuous upward trend in recent years[35]. According to relevant studies, carbon emissions in Ningxia increased from 51.7 million tons in 2005 to 225.9 million tons in 2020, and the per capita CO_2 emissions are approximately 31.3 tons[36]. In 2021, the energy consumption per unit of GDP in Ningxia was four times the national average[37].According to the economic and energy development plans of the Ningxia region, it is difficult for its industrial structure, economic structure, and energy structure to break away from the reliance on coal and energy in the short term, which brings great pressure on carbon emission control in the region. As mentioned earlier, CCUS technology is now widely recognized worldwide as an indispensable strategic technology for building a zero-carbon energy system, promoting zero-carbon industrial processes, providing additional emission space, safeguarding the stable development of the economy and society, and achieving the carbon neutrality goal. Therefore, geological storage of carbon dioxide in this region is imminent. Some scholars, using the CO_2 geological storage capacity calculation method proposed by the Carbon Sequestration Leadership Forum (CSLF), believe that the geological storage potential of CO_2 in Ningxia is considerable, with a theoretical storage capacity of up to 15.155 billion tons, of which the theoretical storage capacity of CO_2 in deep unmineable coal seams is 191 million tons[38]. Thus, it is imperative to conduct a feasibility evaluation of geological storage of carbon dioxide in the unmineable coal seams of the Ningxia region.

This study takes the coal seams of the Jurassic Yan'an Formation in the Ningxia region as the research object and systematically carries out experiments on the interaction of CO_2-water-coal. The study aims to deeply explore the characteristics of pore structure changes in the coal seams of this region after contact with supercritical CO_2, and to reveal the migration process and patterns of trace elements released from the coal seams under the leaching action of supercritical CO_2. This study has important scientific significance and practical value for the achievement of the "dual carbon" goals in Ningxia region.

2.Geological setting

The Ningxia Region is located in the northwest inland of China, bordering Shaanxi to the east, Gansu to the south, and Inner Mongolia to the northwest. In terms of tectonics, it is situated in the middle and southern part of the Qaidam–North China Plate, at the junction of the North China Block, the Alxa microcontinent, and the Early Paleozoic Qilian orogenic belt. It serves as a pivotal region connecting the different tectonic units of western and eastern northern China and is also an important boundary area for China's stratigraphy, tectonics, geomorphology, and various geophysical fields. The unique geological tectonic conditions have given rise to Ningxia's characteristic of having abundant coal resources within a relatively small area[36].

The Ningxia region contains Paleozoic, Mesozoic, and Cenozoic strata. The Paleozoic strata are extensively covered and deeply buried beneath the widely developed Mesozoic and Cenozoic strata. The stratigraphic sequence from which samples were collected in this study, from oldest to youngest, includes the Upper Triassic Shangtian Formation (T_{3s}); the Middle Jurassic Yan'an Formation (J_{2y}), Zhi Luo Formation (J_{2z}), and the Upper Jurassic Anding Formation (J_{3a}); the Eocene (E), and the Quaternary (Q). Among these, the Middle Jurassic Yan'an Formation (J_{2y}) is the primary coal-bearing stratum in the study area. The depositional environments can be categorized into two major types: shallow lacustrine deltaic systems and fluvial systems, with the former being predominant. Within the shallow lacustrine deltaic system, sub-environments such as delta plain, delta front, and prodelta–shallow lake facies can be distinguished. The fluvial system, which is of secondary importance, includes sub-environments such as channel, floodplain, and overbank swamp facies. Drilling wells have revealed a maximum thickness of 399.38 m, a minimum thickness of 303.27 m, and an average thickness of 335.37 m for this formation. The lithology consists of gray and light gray feldspathic quartz sandstone, dark gray and grayish-black siltstone, mudstone, coal, and minor aluminous mudstone（Figure 1）. The base of the formation is in paraconformable contact with the underlying Upper Triassic Shangtian Formation (T_{3s}), marked by a set of coarse-grained sandstone and conglomeratic sandstone with light white or yellowish hues and red spots. The principal lithological characteristics of the Middle Jurassic Yan'an Formation are illustrated in Figure 1. Additionally, based on the lithological filling characteristics of the strata (with coarser coal-bearing clastic fillings in the upper and lower parts of the coal-bearing strata, and finer coal-bearing clastic fillings in the middle part), the coal-bearing strata of the Yan'an Formation are divided into five sections(S1-S5)(Figure 1).

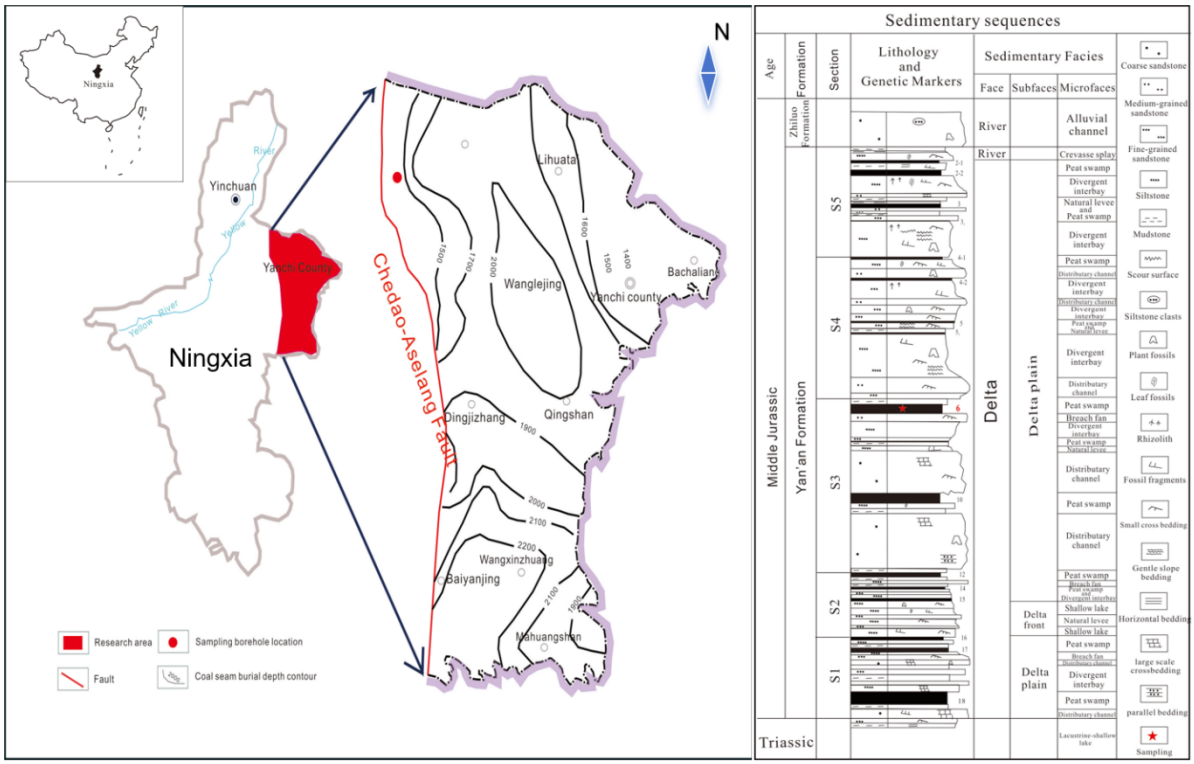

Figure 1. Location and sedimentary sequences of study area, and the locations of the studied samples in this study. (modified by Li et al.[39])

3.Samples and methods

3.1 Samples

This study selected the No. 6 coal at the top of the third section （S3) as the research object and named the samples 6M（Figure 1）. The industrial analysis of the coal samples was conducted according to the ASTM （American Society for Testing and Materials）standards D3175-02, D3174-04, and D3173-03. Meanwhile, the samples were prepared in accordance with the ASTM standard D2797－04, and then subjected to microscopic analysis under reflected light. The fundamental characteristics of the 6M is presented in Table 1. The analytical results indicate that the organic components account for 90.3% of the total coal sample, among which the vitrinite content is 44.3%, the inertinite content is 46%. Its moisture content is 4.72%. The inorganic components account for 4.6% of the total coal sample, with clay minerals contributing 3.6%, carbonate minerals 0.6%, sulfate minerals 1.1%, and silica 0.3%. The volatile matter content is 30.13%, the carbon content is 78.23%, the hydrogen content is 4.28%, the nitrogen content is 0.87%, and the oxygen content is 14.37%. The maximum vitrinite reflectance (Ro, max) of the 6M is 0.57%, characteristic of non-caking coal .

Table 1. Maximum vitrinite reflectance, total sulfur content, and ultimate and proximate analyses of the 6M

Sample	Ro,max (%)	Vitrinite (Vol.%)	Inertinite (Vol.%)	Proximate analyses (%)			Ultimate analyses (%)				Coal type
				Mad	Ad	Vdaf	C_{daf}	H_{daf}	N_{daf}	O_{daf}	
6M	0.57	44.3	46.0	4.72	4.60	30.13	78.23	4.28	0.87	14.37	Non-caking coal

3.2 Experimental procedure

This study mainly consists of $scCO_2$–water–coal simulation experiments, pore structure characterization, trace element testing of solid samples, and element analysis of reaction solutions. The experimental procedure is illustrated in Figure 2, and the specific operational steps are described as follows:

3.2.1 $ScCO_2$–water–coal simulation experiment

This experiment takes coal rock sample 6M as the simulation object. According to the historical data of coalfield drilling in the study area, the temperature range at a burial depth of 1000 m is 35.27–47.30°C, and the pressure range is 7–9 MPa. Based on this information, the experiment simulates the stratum environment at a burial depth of 1000 m, with the experimental temperature set at 40°C and the experimental pressure at 9 MPa. To accelerate the reaction process and reduce the impact of sample heterogeneity on the experiment, the original samples were crushed to 10–20 mesh (particle size approximately 0.84–2.00 mm). Deionized water was used in place of formation water to eliminate the interference of pre-existing ions in the formation water, ensuring that the ions detected in the solution after the reaction mainly originated from the dissolution of minerals in the coal. The experiment was set with a mass ratio of coal sample to deionized water of 10:1 (water/coal), and the reaction times were 1, 3, 5, and 7 days, with a total of four experimental groups.Therefore, in this experiment, the sample that is not subjected to $scCO_2$ simulation is named 6M-0, while the samples subjected to simulation experiments for 1, 3, 5, and 7 days are respectively named 6M-1, 6M-3, 6M-5, and 6M-7.

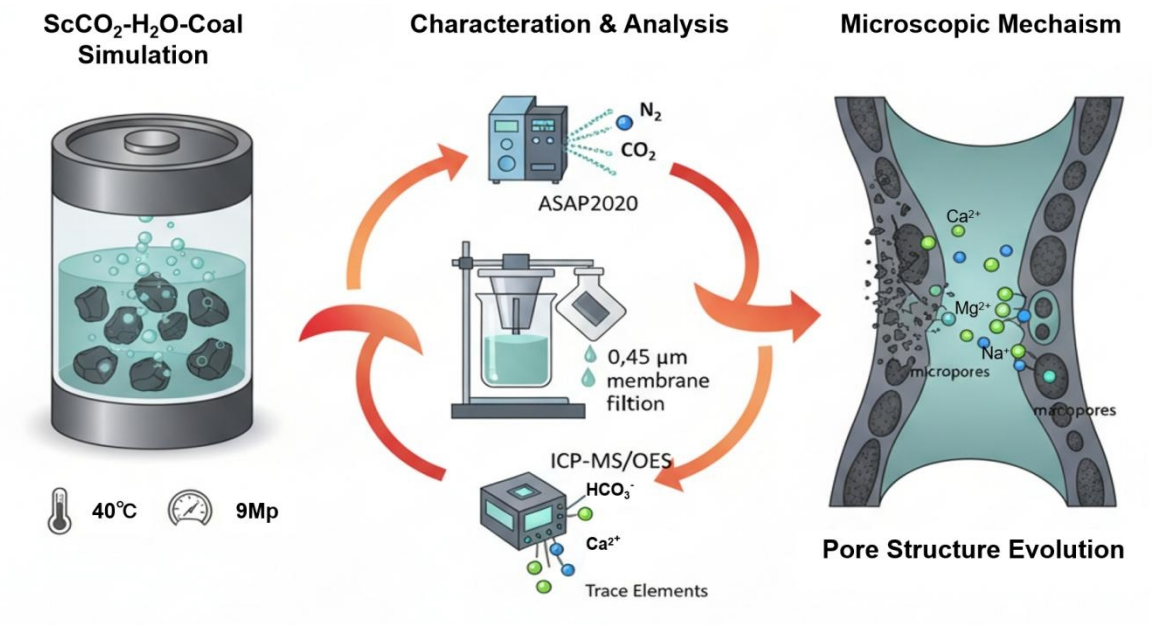

Figure 2. Experimental equipment and workflow

The experimental apparatus used for the underground CO_2 storage simulation process was a high-temperature and high-pressure thermal simulation reactor. Prior to each experiment, the reactor was soaked in concentrated hydrochloric acid to clean the vessel body, followed by repeated rinsing with deionized water to thoroughly remove any residual acid and prevent contamination. Meanwhile the experimental samples were subjected to drying in an oven at 100℃ for 10 hours to remove free water from the samples, thereby establishing a baseline for the samples.

In accordance with the experimental design, the high-temperature and high-pressure simulation experiments for the corresponding coal rock samples were terminated at 1, 3, 5, and 7 days, respectively. After the experiments were concluded, the simulated samples were removed, and the solution pH was immediately measured using a calibrated pH meter. The concentration of HCO_3^- was determined by standard solution titration. Subsequently, the reaction solution was filtered through a 0.45 μm filter membrane and acidified to pH 2 with a 3% (by mass) HNO_3 solution to suppress the formation of carbonate precipitates. The treated reaction solution was then sealed in high-density polyethylene (HDPE) plastic bottles and sent for analysis within 24 hours to ensure the accuracy of the test results. The solid samples were dried in an oven at 40°C for 48 hours before being sent for analysis.

3.2.2 Pore structure analysis

The characterization of the pore structure of solid samples before and after the simulation experiments was conducted using low-temperature N_2 and CO_2 gas adsorption.

The low-temperature gas adsorption experiments were primarily performed using an ASAP2020 surface area and porosity analyzer produced by Micromeritics (USA) (Figure 2). It provides quantitative assessments of specific surface area, pore volume, and pore size distribution. During the experimental process, the samples were first crushed and sieved to 60–80 mesh, then subjected to vacuum drying at 110°C for 12 hours to thoroughly remove residual moisture and volatile components. The dried samples were then subjected to low-temperature N_2 and CO_2 adsorption experiments. The low-temperature N_2 adsorption experiment was conducted at -196°C (liquid nitrogen temperature) with a relative pressure (P/P_0) range of 0.001–0.998. The specific surface area, pore volume, and pore size distribution parameters are typically calculated based on the N_2 adsorption branch curve. The BET model (Brunauer-Emmett-Teller) was used to calculate the specific surface area, while the BJH model (Barrett-Joyner-Halenda) was used to calculate the total pore volume, average pore size, and pore size distribution. The low-pressure CO_2 adsorption experiment was conducted at 0°C with a relative pressure (P/P_0) range of 0.00003–0.03, and the DFT model (Density Functional Theory) was used to calculate the micropore volume, micropore specific surface area, and micropore size distribution.

3.2.3 Elemental analysis

The measurement of trace elements in solid samples before and after the simulation experiment was conducted using a Nu Attom laser ablation inductively coupled plasma mass spectrometer (LA-ICP-MS) produced by N.U. Instruments in the UK . The sample pretreatment involved acid dissolution. First, samples with a particle size less than 200 mesh were dried for approximately 3 hours at 105°C to remove moisture and ensure accurate weighing. Then, 50±1 mg of rock sample was weighed and placed into a PTFE digestion vessel, followed by the addition of HNO_3, HF, and $HClO_4$ to dissolve the sample. Finally, a Rh internal standard solution was added and the mixture was diluted to 100.0 g with deionized water, resulting in a Rh concentration of 10 ng/mL in the solution, which was then ready for testing.

The elemental analysis of the reaction liquid was performed using an Optima 8000 inductively coupled plasma optical emission spectrometer (ICP-OES) produced by PerkinElmer in Germany. This instrument generates a plasma using a high-frequency induction coil to vaporize the sample and excite the elements to emit light. The characteristic spectra are separated by the optical system and detected by a photomultiplier for both qualitative and quantitative analysis. The standard sample used was River Thames.

4.Results and discussion

4.1 Elements migration

The forms of elements in coal are diverse, mainly including combination with organic matter, occurrence in the mineral components of coal, adsorption on the surface of coal, and existence in the form of ions in the pore water of coal[40,41,42]. In addition to the major elements such as C, H, S, N, and O, the elements combined with the organic matter of coal also include some trace elements and specific metal elements, such as Ge, V, Zn, Cu, Ga, U, while elements like Be, Ti, Nb, Ta, and Hf may also have varying degrees of organic affinity[41,42,43]. Minerals are important carriers of elements in coal[44]. The elements associated with minerals include Si, Al, Fe, Ca, Mg, K, Na, Ti, Mn, Zn, Cu, Co, Ni, Li, Be, V, Cr, Pb, U, Ga, Sr, etc. These elements primarily form silicates, oxides, sulfides, carbonates, phosphates, and other minerals in coal. Common minerals include quartz, feldspar, clay minerals, calcite, and dolomite. Moreover, these minerals have a strong adsorption capacity for certain elements[45,46].

As previously reported, after CO_2 is injected into coal seams, it forms an acidic fluid with the water in the coal seams[47,48]. This is because, after CO_2 injection, it dissolves in water to form carbonic acid, which then rapidly decomposes into bicarbonate ions, generating a large number of H^+ ions. The reaction processes are shown in Equations (1) and (2):

$$CO_2+H_2O \rightleftarrows H_2CO_3 \quad (1)$$

$$H_2CO_3 \leftrightharpoons H^+ + HCO_3^- \quad (2)$$

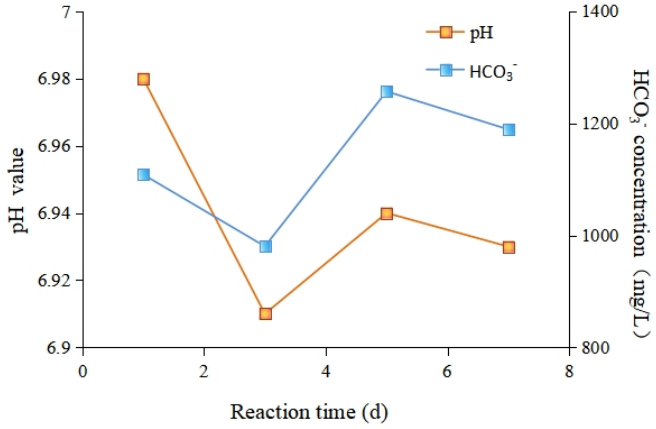

Figure 3. HCO_3^- and pH profiles in the reaction solution for each simulated experiment

After each simulation experiment, the pH and bicarbonate ion concentration of the experimental solution were measured （Figure 3）. The results were consistent with the

aforementioned reaction process, i.e., the formation of an acidic fluid from carbon dioxide and water.

This acidic fluid undergoes geochemical reactions with the minerals and organic matter in the coal seams, leading to changes in the minerals and organic matter[44,49,50]. This process is primarily characterized by two distinct features: (1) The dissolution of major elements(e.g., Si, Al, Fe) and trace elements (e.g., As, Pb, Cd) results in the disruption of mineral crystal structures; (2) Elements in various occurrence forms (including ion-exchangeable, carbonate-bound, and iron-manganese oxide-bound forms) exhibit differential migration behaviors within the CO_2-water-coal interaction system[48,51]. During the process of activation and release of elements contained in the minerals and organic matter, the quantity and structure of the minerals and organic matter also change, and the elements adsorbed on the surfaces of the organic matter and minerals are also mobilized. When the injection reaches a certain depth, the temperature and pressure exceed the critical temperature and pressure of CO_2. Due to the unique properties of scCO_2, the migration of elements in the coal seams becomes more pronounced[52,53]. This geochemical redistribution process of elements not only reflects the mechanisms of CO_2 - coal interactions but also provides important indicators for assessing the long - term stability of the storage system.

4.1.1 Reactive liquid analysis

As described in the experimental methods, the water injected in this experiment is deionized. Therefore, the leachate after the reaction represents the elemental characteristics of the water in the coal seam after CO_2 sequestration, that is, the elements that may be released from coal after exposure to supercritical CO_2. The detection results of the reaction solution are shown in Table 2 and Figure 4.

Table 2. The concentration of elements in each experimental reaction solution（ppm）

Element types	Sample	Ca	Na	Mg	K	Si	Al	Fe	Mn
major elements	6M-1	312.411	55.496	22.938	1.042	0.636	0.301	0.027	1.541
	6M-3	228.583	55.278	21.947	1.035	0.656	0.257	0.029	1.184
	6M-5	366.604	51.873	25.804	1.402	1.364	0.075	0	1.364
	6M-7	349.689	58.393	23.059	1.054	2.398	0.041	0	1.354

Element types	Sample	B	Ba	Be	Cr	Cu	Ga	Li	Ni	Pb	Rb	Sr	Ti	V	Zn

	6M-1	1.675	0.599	0.155	0.066	0.098	0.528	0.285	1.328	0.072	1.168	2.086	0.089	0.078	0.047
trace	6M-3	1.832	0.616	0.062	0	0.155	0.433	0.133	0.143	0.030	1.780	1.825	0.183	0	0
elements	6M-5	2.571	0.568	0.237	0	0.052	0.255	0.152	1.021	0	1.218	2.085	0.029	0	0
	6M-7	2.236	0.409	0.237	0	0.053	0.259	0.151	0.686	0	1.232	1.884	0.028	0	0

Figure 4. Ion concentrations in the reaction solution versus experimental time

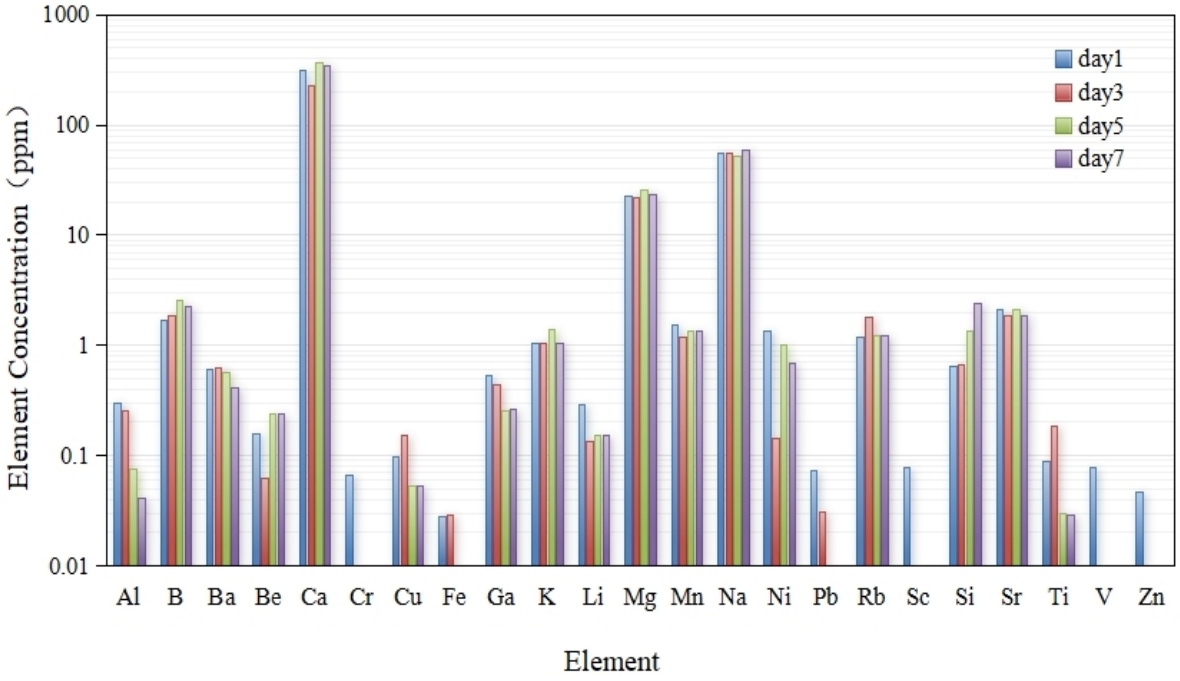

The experimental results indicate that the major element with the highest measurable concentration in the reaction solution is Ca, with a minimum content of 228.6 ppm and a maximum of 366.6 ppm across all reaction solutions. The next most abundant elements are Na (50-60 ppm) and Mg (20-30 ppm). The concentrations of all other detected elements are below 3 ppm. The Si concentration exhibited a sustained increasing trend (from 0.64 to 2.40 ppm), implying the slow dissolution of silicate.The Al concentration exhibited a continuous decreasing trend (from 0.30 ppm to 0.04 ppm).The content of Fe is the lowest, and its concentration is even zero in the 5-day and 7-day simulation experiments,which may be attributed to the precipitation of secondary minerals. In addition, 14 trace elements are detected in the reaction solution, all with relatively low concentrations. Elements such as Cr, Pb, V, and Zn are detected in the 1-day and 3-day experiments, but their concentrations are zero in the 5-day and 7-day experiments.

4.1.2 Migration of trace elements in coal

During the geological storage of CO_2, the interaction between water and CO_2 renders the formation water acidic, which has a transformative effect on minerals[48,51]. This process can lead to the leaching of numerous major and trace elements from coal into the aqueous solution，and as a result, the minerals and elements within the coal also undergo changes. The occurrence and concentration of trace elements in coal are important factors that determine the extent of their migration and transformation. In this study, the 6M and the other four samples subjected to supercritical CO_2 injection simulation experiments are tested for trace element content, with a total of 20 trace elements being detected (Table 3 and Figure 5).

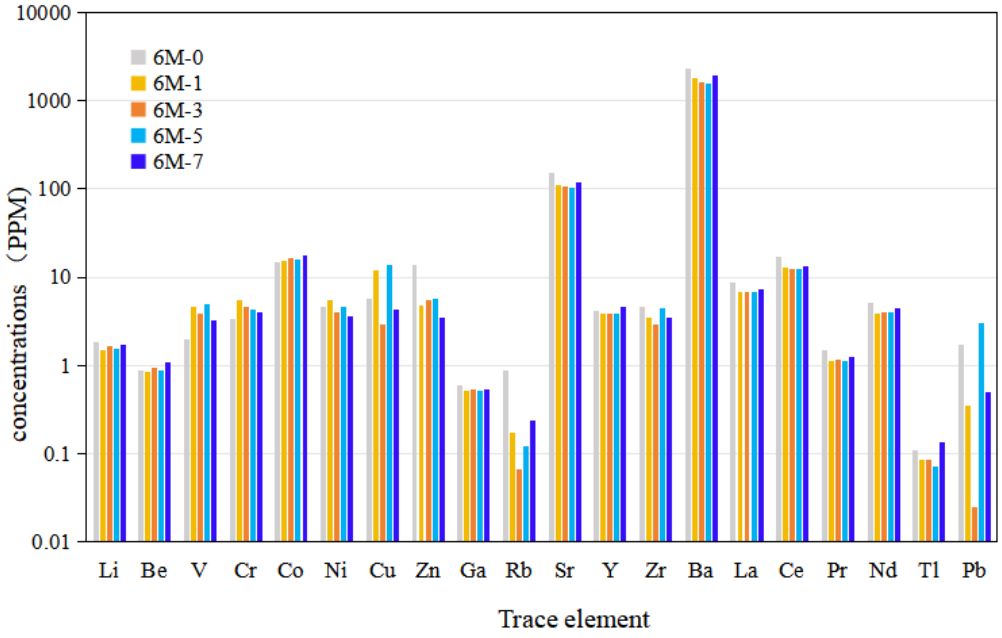

Figure 5. Variations of trace element concentrations in raw coal and simulated coal samples

Table 3. The concentrations of trace elements in raw coal and coal samples after each group of experiments（ppm）

Sample	Li	Be	V	Cr	Co	Ni	Cu	Zn	Ga	Rb	Sr	Y	Zr	Ba	La	Ce	Pr	Nd	Tl	Pb
6M-0	1.838	0.892	2.015	3.347	15.031	4.608	5.632	13.741	0.593	0.881	153.779	4.102	4.615	2331.246	8.768	16.913	1.516	5.147	0.111	1.751
6M-1	1.487	0.840	4.681	5.552	15.455	5.618	12.026	4.765	0.512	0.176	112.517	3.850	3.435	1790.545	6.873	12.733	1.120	3.882	0.085	0.349
6M-3	1.667	0.941	3.841	4.569	16.702	3.963	2.969	5.556	0.532	0.067	107.550	3.919	2.933	1623.313	6.946	12.560	1.162	4.075	0.085	0.025
6M-5	1.535	0.891	4.991	4.274	15.884	4.631	13.856	5.729	0.511	0.124	104.501	3.865	4.462	1588.977	6.717	12.276	1.126	3.954	0.072	3.068
6M-7	1.706	1.084	3.216	4.082	17.753	3.620	4.298	3.550	0.540	0.236	119.737	4.571	3.521	1906.107	7.426	13.508	1.247	4.443	0.134	0.510

Table 4. The migration rate of trace elements in the coal sample after the experiment（%）

Sample	Li	Be	V	Cr	Co	Ni	Cu	Zn	Ga	Rb	Sr	Y	Zr	Ba	La	Ce	Pr	Nd	Tl	Pb
6M-1	-19.08	-5.83	132.37	65.90	2.82	21.91	113.53	-65.32	-13.75	-80.08	-26.83	-6.17	-25.56	-23.19	-21.62	-24.71	-26.15	-24.57	-23.61	-80.07
6M-3	-9.28	5.44	90.65	36.53	11.12	-14.00	-47.28	-59.56	-10.32	-92.35	-30.06	-4.47	-36.45	-30.37	-20.78	-25.74	-23.39	-20.83	-23.94	-98.57
6M-5	-16.48	-0.11	147.75	27.71	5.67	0.49	146.03	-58.30	-13.87	-85.96	-32.04	-5.79	-3.30	-31.84	-23.39	-27.42	-25.70	-23.19	-34.84	75.18
6M-7	-7.20	21.51	59.62	21.97	18.11	-21.45	-23.69	-74.17	-9.00	-73.19	-22.14	11.41	-23.70	-18.24	-15.31	-20.13	-17.72	-13.68	20.82	-70.91

The “-” preceding the values in the table indicates that the element concentration in the sample after the experiment is lower than that in the sample before the experiment.

Meanwhile, the migration rate of elements is also calculated as follow:

$$\text{Migration rate (\%)} = (N_i - N_0)/N_0 \times 100\%$$

where N_i is the concentration of a given element after the simulation experiment on day i, and N_0 is the concentration of the same element in the 6M sample before the experiment. The calculation results are presented in Table 4 and Figure 6.

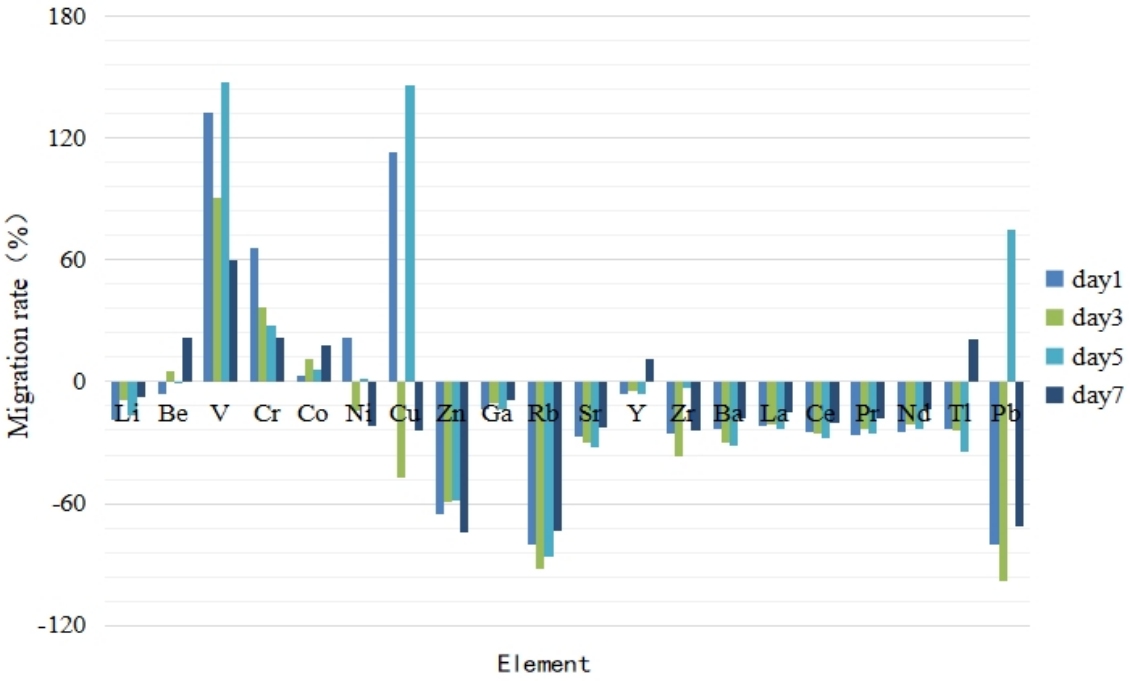

Figure 6. Element mobility

Based on the test results, the 20 detected trace elements were classified into four migration groups: (1) Highly migratory elements. Rubidium (Rb), zinc (Zn), and lead (Pb) exhibited sharp concentration declines after one day of reaction, with maximum release rates of 92.4%, 74.2%, and 98.6%, respectively. The Rb concentration decreased from an initial value of 0.881 ppm to a range of 0.067–0.236 ppm, making Rb the most sensitive element in this experiment. Pb release displayed strong heterogeneity: its concentration dropped to 0.025 ppm after 3 days of reaction yet abnormally rose to 3.068 ppm after 5 days, which was 75% higher than the initial concentration. This phenomenon implies a pronounced local re-precipitation process. (2) Moderately migratory elements. Strontium (Sr), barium (Ba), and light rare earth elements (LREEs, La–Nd) showed a continuous decreasing trend, with net release rates of 22.2%, 18.2%, and 20.3%–24.5%, respectively, after 7 days of reaction. The release rates of the four light rare earth elements exhibited strong consistency, with a coefficient of variation below 10%, indicating their congruent release from an identical host phase. (3) Fluctuating elements. Copper (Cu), nickel (Ni), vanadium (V), and chromium (Cr)

displayed drastic temporal fluctuations without any monotonic variation trend. The concentration of Cu increased by 114% after 1 day of reaction and then decreased by 75% at day 3. By contrast, V and Cr concentrations rose overall throughout the reaction process, with maximum relative increments of 147% and 66%, respectively. (4) Stable elements. Cobalt (Co) and beryllium (Be) varied by less than 15% throughout the entire reaction period, which suggests that these two elements are predominantly hosted within stable mineral lattices.

4.1.3 Element migration and the safety of $scCO_2$ storage in the study area

The released elements not only alter the coal seam's internal architecture but also migrate along cleats within the coal matrix and through artificially induced hydraulic fractures. These trace elements that were once sequestered in deep coal seams will pose a significant pollution risk to shallow aquifers, surface water bodies and the soil as they migrate. Based on the severity of their environmental impacts, the elements can be classified into four distinct categories:1. Elements exhibiting the most pronounced environmental hazards, exemplified by As, Cd, Cr, Hg, and Se. 2. Elements associated with secondary environmental concern, including B, Cl, F, Mn, Mo, Ni, and Pb. 3.Elements of comparatively limited environmental impact, such as Be, Cu, P, Th, V, and Zn. 4. Elements entailing the lowest environmental risk, namely Ba, Co, Sb, Sn, and Tl[54].

Table 3 reports the trace-element analyses of coal samples before and after the $scCO_2$ simulation experiments, and Table 4 summarizes the corresponding element-specific migration rates. The data show that only V, Cr and Co exhibit higher concentrations after $scCO_2$ exposure; the remaining elements display both increases and decreases relative to their initial contents (Figure 3). Previous studies attribute this variability to $scCO_2$-induced extraction of mineral phases and organic functional groups. Such interactions can induce mineral recrystallization or structural collapse and can cleave or rearrange organic moieties, thereby enlarging existing pores or generating new ones[55]. Consequently, elements become either more accessible for detection or more prone to loss, which collectively drives the observed fluctuations in elemental inventories. However, a rigorous assessment of the safety of geological CO_2 sequestration should rely primarily on the elemental determinations in the post-experiment reaction solution(Table 2), because only those elements that partition into the formation water pose a plausible risk of contaminant migration. Table 2 indicates that the potentially hazardous elements detected in the reacted solutions are Cr, Pb, Cu, Zn, and Ti. With reference to the Environmental Quality Standards for Surface Water, only Cu marginally exceeds the regulatory limit of 0.05 ppm. Specifically, Cu concentrations were

markedly elevated on days 1 and 3, whereas on days 5 and 7 they remained only slightly above the threshold. These results demonstrate that the coal–$scCO_2$–H_2O interaction mobilized only trace quantities of these elements, implying a comparatively low environmental hazard. Nevertheless, continued monitoring of these specific elements in the target formation remains imperative.

4.2 Pore changes

4.2.1 Gas adsorption curves

The low-temperature N_2 and CO_2 gas adsorption curves of 6M and its samples after $scCO_2$ simulation experiments are shown in Figure 7. The pore volume, specific surface area, and maximum adsorption capacity calculated based on the gas adsorption model are presented in Table 5. According to the shape of the physical isothermal adsorption curves and the hysteresis loop characteristics as well as the N_2 adsorption curves (Figure 7a), it is concluded that 6M mainly develops slit-like meso-macropores and ink-bottle mesopores[56]. In addition, as described by Sing (1985), the non-coincidence of adsorption and desorption curves at lower pressures in the N_2 adsorption curves is due to the presence of a large number of micropores in the samples, which prevent the adsorbed gas from being rapidly desorbed after entering the pores[56]. The adsorption curves of the original 6M sample (6M-0) and the $scCO_2$ simulation samples (except for 6M-5) do not close at relatively low pressures (0–0.5), indicating the development of micropores in the coal samples. This is also confirmed by the CO_2 adsorption results (Figure 7b, Table 5), which show that all samples have well-developed micropores. However, in comparison, the nitrogen adsorption and desorption curves of the samples simulated by $scCO_2$（6M-1~6M-7) have a higher degree of closure compared to the 6M-0 (Figure 7a)， that indicates that after being soaked in supercritical carbon dioxide, the connectivity of the micropores in 6M is improved.

In addition, as shown in Figure 7a and Table 5, after the $scCO_2$ simulation experiment, the specific surface area calculated by the BET method, the pore volume calculated by the BJH method, and the maximum adsorption capacity of 6M all show a general trend of continuous decline. In contrast, the pore diameter calculated by the BJH method exhibits an upward trend. However, the CO_2 gas adsorption capacity, specific surface area, and pore volume of 6M after the $scCO_2$ simulation experiment were significantly enhanced (Figure 7b and Table 5).

(a)

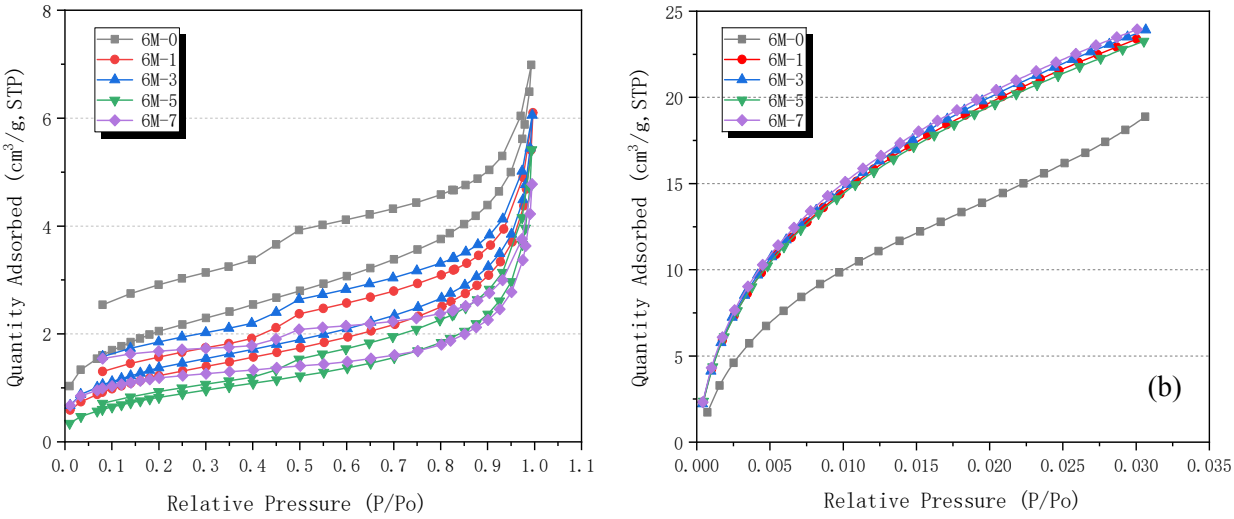

Figure 7. The gas adsorption curves of 6M before and after the experiment.(a):N_2 adsorption curves, (b):CO_2 adsorption curves

Table 5. The basic data of gas adsorption of 6M before and after the experiment

Sample	N_2 adsorption				CO_2 adsorption		
	BET superficial area (m²/g)	BJH pore volume (cm³/g)	BJH pore diameter (nm)	maximal adsorption capacity (cm³/g, STP)	DA superficial area (m²/g)	DA pore volume (cm³/g)	maximal adsorption capacity (cm³/g, STP)
6M-0	7.2587	0.010845	6.072	6.9868	184.879	0.079	18.873
6M-1	4.491	0.008	7.899	6.097	211.725	0.087	23.389
6M-3	4.919	0.009206	7.9505	6.0533	214.387	0.088	23.914
6M-5	3.1209	0.008096	11.3015	5.4170	203.933	0.083	23.258
6M-7	3.9207	0.006875	9.8657	4.7767	211.345	0.086	23.945

4.2.2 Variation of specific surface area

This study presents the distribution characteristics of specific surface area with pore size changes calculated by the BJH model for N_2 adsorption, as well as those calculated by the DFT model for CO_2 adsorption. The pore sizes calculated from N_2 adsorption range from 1.74 to 300 nm, while those calculated from CO_2 adsorption range from 0.47 to 1.083 nm. Therefore, the distribution characteristics of specific surface area with pore size in gas adsorption for the samples of 6M before and after simulation were spliced, and the results are shown in Figure 8.

Figure 8 shows results consistent with previous studies, that is, the specific surface area of coal is mainly contributed by pores smaller than 10 nm. Additionally, Table 5 provides the

basic characteristics of specific surface area changes in this simulation experiment, that is, after the $scCO_2$ simulation experiment, the specific surface area of 6M calculated by N_2 gas adsorption decreases, while the specific surface area calculated by CO_2 adsorption increases. Through data splicing, it is possible to more finely observe the changes in pore characteristics of 6M after the $scCO_2$ simulation experiment, that is, pores smaller than 1 nm have a more extensive distribution after the $scCO_2$ simulation experiment, while pores between 1 and 10 nm continuously decrease.

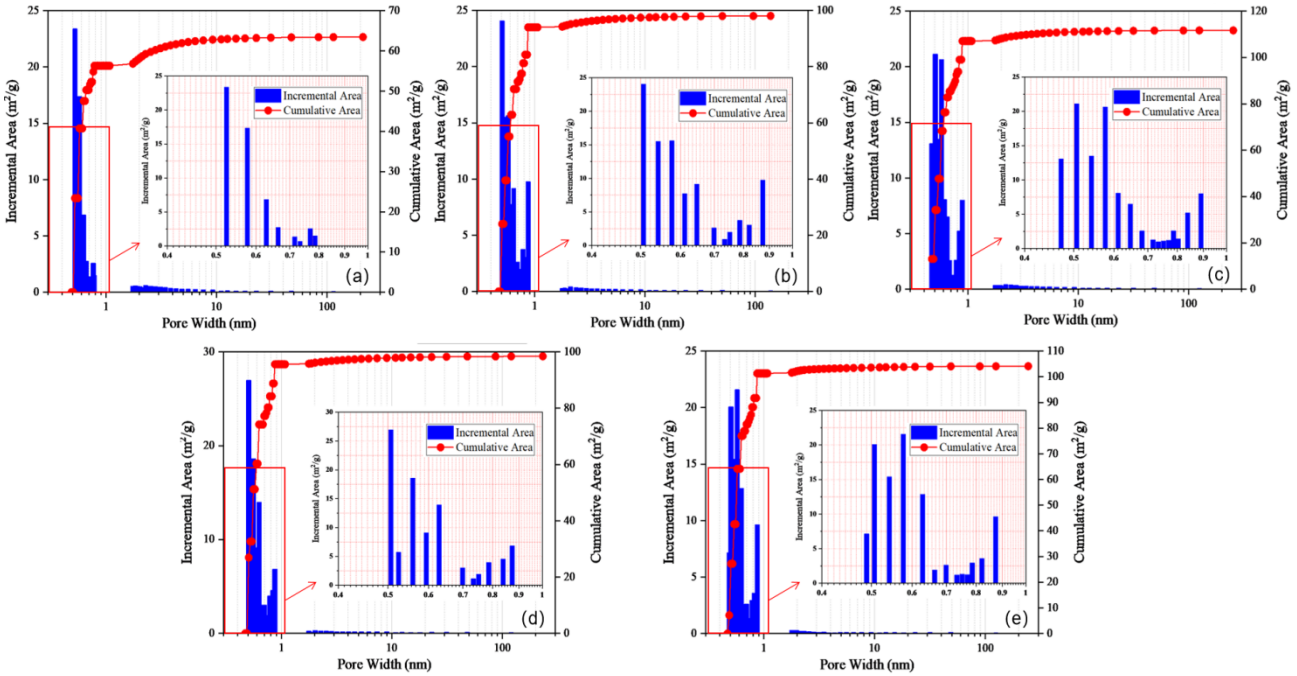

Figure 8. The specific surface area distribution of 6M before and after the experiment based on the N_2 and CO_2 adsorption. (a) is for 6M-0, (b) is for 6M-1,(c) is for 6M-3,(d) is for 6M-5,(e) is for 6M-7.

4.2.3 Variation of pore volume

Similarly, the distribution data of pore volume with pore size for gas adsorption were also spliced in the same manner as the specific surface area data, and the splicing results are shown in Figure 9. Figure 9 shows that the trend of pore volume changes for pores smaller than 10 nm in 6M is consistent with the trend of specific surface area changes, that is, pores smaller than 1 nm increase after the $scCO_2$ simulation experiment, while pores between 1 and 10 nm decrease.In addition, the pore volume distribution curve also reveals the characteristics of pores larger than 10 nm in 6M after the $scCO_2$ simulation experiment: pores in the range of 10–50 nm decrease after the simulation experiment, while pores larger than 50 nm increase slightly.

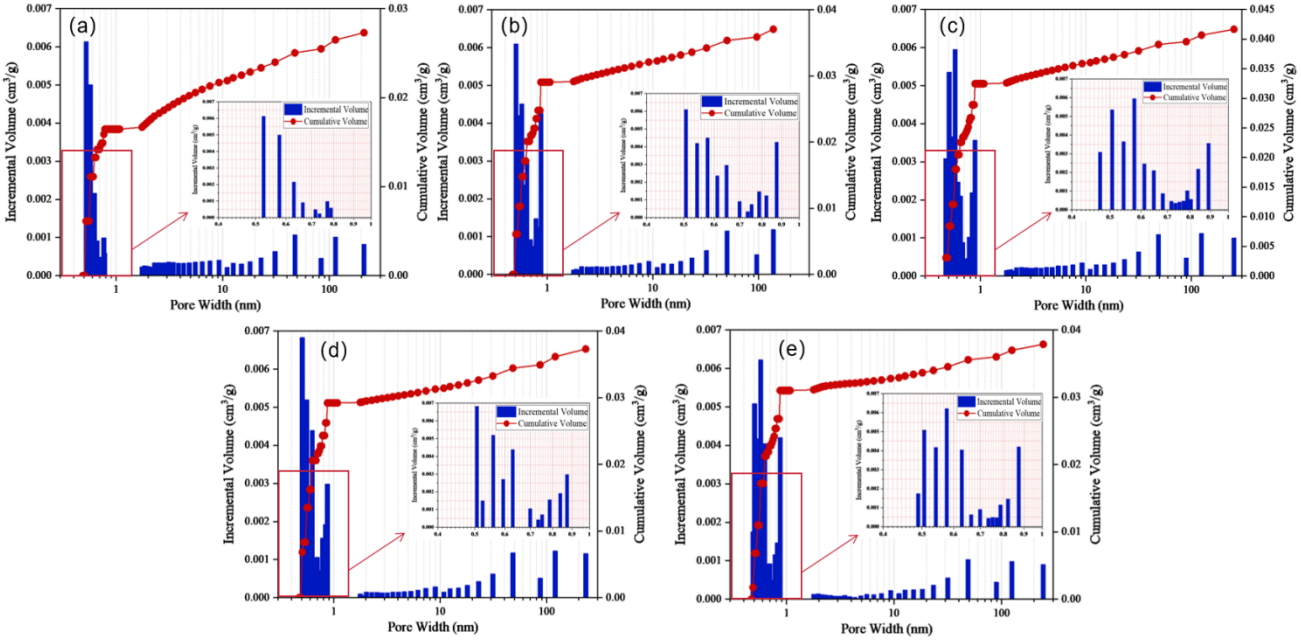

Figure 9. The hole volume distribution of 6M before and after the experiment based on the N_2 and CO_2 adsorption. (a) is for 6M-0, (b) is for 6M-1,(c) is for 6M-3,(d) is for 6M-5,(e) is for 6M-7.

4.2.4 Evolution of pore structure and element migration in coal reservoirs

In this study, both the 6M sample and the samples subjected to $scCO_2$ simulation experiments underwent low-temperature N_2 and CO_2 gas adsorption experiments. The basic data of the two experiments for the five samples are shown in Table 5. As can be seen from the table, the N_2 adsorption capacity of 6M, the specific surface area calculated by the BET model, and the pore volume calculated by the BJH model all decreased significantly with the increase of simulation time. In contrast, only the pore diameter calculated by the BJH model increased to a certain extent with the increase of simulation time. Compared with the original sample, the CO_2 adsorption capacity of the samples subjected to $scCO_2$ simulation experiments, as well as the specific surface area and pore volume calculated by the DA model, were all enhanced. However, their changes were not significantly related to the duration of the simulation. In addition, this study has concatenated the distribution characteristics of specific surface area and pore volume of two gas adsorptions for five samples with respect to pore size. The results of the concatenation are shown in Figures 8 and 9. The results indicate that for the 6M sample after the $scCO_2$ simulation experiment, the micropores less than 1 nm significantly increased, the micropores and mesopores in the range of 1–50 nm continuously decreased, and the macropores larger than 50 nm slightly increased. Previous studies have shown that micropores are the primary sites for gas adsorption[57,58].

The results of gas adsorption indicate that after being soaked in supercritical carbon dioxide, the micropores in 6M are more developed. Therefore, it is concluded that the coal rocks in the study area are conducive to carbon dioxide sequestration. Moreover, after sequestration, more micropores can be generated, which in turn enhances the capacity for carbon dioxide adsorption.

CO_2 is an "active gas" that is soluble in water. When CO_2 is injected into deionized water, the pH value of the deionized water becomes weakly acidic. As the temperature and pressure increase, CO_2 becomes a supercritical fluid, which is an excellent solvent. It can penetrate into the pore structure of coal, dissolve the small-molecule organic matter and soluble minerals within, thereby altering the composition and structure of coal[55,59,60,61].

In this experiment, the major elements measured in the reaction solution were Ca (highest), followed by Na, Mg, and K, with minor amounts of Mn, Si, Al, and Fe also detected (Table 2). These results are consistent with the findings of Li et al. (2023) and Chen et al. (2023)[47,48]. In the weakly acidic system of $scCO_2$-H_2O, carbonate minerals such as calcite and dolomite are highly susceptible to dissolution (equations (1) – (4))[55,59,60].

$$CaCO_3+H^+\rightarrow Ca^{2+}+HCO_3^- \quad (1)$$

$$CaCO_3+H_2CO_3\rightarrow Ca^{2+}+2HCO_3 \quad (2)$$

$$Ca(Fe_{0.7}Mg_{0.3})(CO_3)_2+2H^+\rightarrow Ca^{2+}+0.7Fe^{2+}+0.3Mg^{2+}+2HCO_3^- \quad (3)$$

$$CaMg(CO_3)_2+2H^+\rightarrow Ca^{2+}+Mg^{2+}+2HCO_3^- \quad (4)$$

Furthermore, in the presence of Mg, the solubility of calcite is enhanced. Therefore, when both minerals are present, calcite dissolves more readily than dolomite, resulting in a higher mobility of Ca compared to Mg. Na is also highly soluble in water , which is primarily found in albite and chlorite. Additionally, the other elements exhibit a certain degree of solubility in the weakly acidic fluid[60,61,62], leading to varying degrees of dissolution of the minerals in this experiment. Of course, other trace elements were also detected in the reaction solution (Table 2). In the absence of supercritical CO_2 extraction, these trace elements primarily exist on the surfaces or within the internal lattices of minerals and organic matter through adsorption or isomorphism. Therefore, when $scCO_2$ infiltrates, these trace elements are released, forming intermolecular pores in coal and contributing significantly to the micropore volume[61,63]. The reduction in mesopores is likely due to the swelling of coal caused by the infiltration of CO_2 solution, which reduces their size, or alternatively, the dissolution process may have interconnected the mesopores to form larger pores.

In addition, numerous scholars have conducted $scCO_2$ simulation experiments on coals of different evolutionary stages and have identified certain patterns. Specifically, low-rank

coals exhibit an increase in micropores and macropores, whereas high-rank coals show a decrease in micropores and an increase in macropores[55,61,63,64]. It is hypothesized that in the low-rank coal stage, the coal internally adsorbs a greater number of elements, which are released due to the extraction effect of $scCO_2$, thereby increasing the micropores. As the maturity of coal increases, these adsorbed elements undergo reorganization or recrystallization under the influence of temperature and pressure, becoming part of minerals or organic matter. Consequently, they are not easily released during $scCO_2$ extraction. Instead, the more highly crystallized soluble minerals are more susceptible to dissolution, resulting in the formation of a greater number of macropores. Does this imply that the more adsorbed elements present, the greater the number of micropores formed during CO_2 sequestration，and as the number of micropores increases, the amount of adsorbed CO_2 also rises?

In reality, however, based on the research findings of numerous scholars, there are many factors that influence the changes in the pore structure of coal during $scCO_2$ simulation experiments, such as the temperature and pressure conditions of the experiment, the saturation level of CO_2 in the fluid, and the initial development of the coal's pore structure. Nevertheless, overall, after the $scCO_2$ simulation experiment, the hazardous elements in the 6M of the study area were found to be extremely low in leaching. Moreover, the CO_2 extraction process increased the microporosity of 6M, which is beneficial for CO_2 sequestration. Therefore, considering these two aspects, the study area is suitable for geological storage of CO_2.

5. Conclusions

This study provides valuable insights into the interaction of $scCO_2$ with coal and water in the Ningxia region, focusing on the changes in pore structure and the migration of trace elements.The following conclusions were drawn through the research：

（1）The interaction between $scCO_2$ and coal leads to the dissolution of major elements (e.g., Ca, Na, Mg) and the mobilization of trace elements (e.g., Cr, Pb, Cu, Zn). However, the concentrations of potentially hazardous elements in the reaction solution are generally low, with only Cu marginally exceeding the regulatory limit for surface water quality. This suggests that the risk of groundwater contamination due to element migration is relatively low under the experimental conditions.

（2）The pore structure of the coal samples undergoes significant changes after exposure to $scCO_2$. The specific surface area and pore volume of micropores (<1 nm) increase, while

the mesopores (1 – 50 nm) decrease. This indicates that the $scCO_2$ enhances the microporosity of the coal, which is beneficial for CO_2 adsorption and storage.Meanwhile, the increase in microporosity is attributed to the dissolution of small-molecule organic matter and soluble minerals by $scCO_2$, which creates new micropores and enlarges existing ones. The reduction in mesopores may be due to the swelling of coal or the interconnection of mesopores to form larger pores.

（3）The study demonstrates that the coal seams in the Ningxia region have the potential for geological CO_2 storage. The increase in microporosity after $scCO_2$ injection enhances the coal's capacity to adsorb CO_2, which is crucial for effective sequestration.The low leaching of hazardous elements suggests that the environmental impact of CO_2 injection on groundwater quality is minimal under the tested conditions. However, continuous monitoring of specific elements (e.g., Cu) is recommended to ensure long-term safety.

Funding

This work was jointly supported by the Key Project of Ningxia Natural Science Foundation (2022AAC02073), Key Research and Development Project of Ningxia Hui Autonomous Region (2024BEG02006).

Conflicts of Interest

The authors declare no conflicts of interest.

References

1. IPCC. Climate Change 2023: Synthesis Report. Contribution of Working Groups I, II and III to the Sixth Assessment Report of the Intergovernmental Panel on Climate Change. Geneva, Switzerland: IPCC, 2023:184.
2. Speech at the 75th General Debate of the United Nations General Assembly by Xi Jingping. People's Daily, 2020-09-23.
3. Gao, X.; Yang,S.; Shen,B.; Tian,L.,Li,S.; Zhang, X.;Wang, J. Influence of reservoir spatial heterogeneity on a multicoupling process of CO_2 geological storage. *Energy & Fuels.* 2023,37(19),14991-15005.[CrossRef]
4. Kumar, M.; Lauderdale-Smith, G. Petrophysical Considerations for CO2 Capture and Storage. *Petrophysics – The SPWLA Journal of Formation Evaluation and Reservoir Description.* 2024, 65(1), 51–69.[CrossRef]
5. Martín, D.; Aparicio, P.; García, S.; Maroto-Valer, M. M. Mixed-Layer Illite-Smectite

Illitization under Supercritical CO_2 Conditions. *Applied Sciences*. 2022,12(22), 11477. [CrossRef]

6. Chen, B.; Li, Q.; Tan, Y., Yu, T.; Li, X.; Li, X. Experimental measurements and characterization models of caprock breakthrough pressure for CO_2 geological storage. *Earth-Science Reviews*. 2024, 252, 104732. [CrossRef]
7. Chen, B.; Harp, D. R.; Zhang, Y.; Oldenburg, C. M.; Pawar, R. J. .Dynamic risk assessment for geologic CO_2 sequestration. *Gondwana Research*. 2022, 122, 232–242.[CrossRef]
8. Luo, J.; Xie, Y.; Hou, M. Z.; Xiong, Y.; Wu, X.; Lüddeke, C. T.; Huang, L. Advances in subsea carbon dioxide utilization and storage. *Energy Reviews*. 2023, 2(1), 100016.[CrossRef]
9. Zhang, Y.; Chu, B.; Huang, T.; Qi, S.; Manga, M.; Zhang, H.; Zheng, B.; Zhou, Y . Using the Tidal Response of Groundwater to Assess and Monitor Caprock Confinement in CO_2 Geological Sequestration. *Water*. 2024,16(6), 868.[CrossRef]
10. Vangkilde-Pedersen, T.; Anthonsen, K.L.; Smith, N.; Kirk, K.; Neele, F.; van der Meer, B.; Le Gallo, Y.; Bossie-Codreanu, D.; Wojcicki, A.; Le Nindre, Y.-M.; Hendriks, C.; Dalhoff, F.; Christensen, N.P. Assessing European capacity for geological storage of carbon dioxide–the EU GeoCapacity project. *Energy Procedia*. 2009, 1, 2663–2670.[CrossRef]
11. White, C. M.; Smith, D. H.; Jones, K. L.; Goodman, A. L.; Jikich, S. A.; LaCount, R. B.; DuBose, S. B.; Ozdemir, E.; Morsi, B. I.; Schroeder, K. T. Sequestration of Carbon Dioxide in Coal with Enhanced Coalbed Methane RecoveryA Review. *Energy & Fuels*. 2005, 19(3), 659 − 724.[CrossRef]
12. Li, C.; Zheng, J.; Huang, S. The effects of supercritical CO_2 on the seepage characteristics and microstructure of water-bearing bituminous coal at in-situ stress conditions. *Frontiers in Earth Science*. 2023,11.[CrossRef]
13. Sun, X.; Wang, H.; Gong, B.; Zhao, H.; Wu, H.; Wu, N.; Sun, W.; Zhang, S.; Jiang, K. . Investigation into Enhancing Methane Recovery and Sequestration Mechanism in Deep Coal Seams by CO_2 Injection. *Energies*. 2024, 17(22), 5659. [CrossRef]
14. Prabu, V.; Mallick, N. . Coalbed methane with CO_2 sequestration: An emerging clean coal technology in India. *Renewable and Sustainable Energy Reviews*. 2015, 50, 229–244.[CrossRef]
15. Perera, M. S. A.; Ranjith, P. G.; Choi, S.K.; Airey, D. Investigation of temperature effect

on permeability of naturally fractured black coal for carbon dioxide movement: an experimental and numerical study. *Fuel.* 2012, 94, 596–605. [CrossRef]

16. Ranathunga, A. S.; Perera, M.S.A.; Ranjith, P. G. Deep coal seams as a greener energy source: a review. *Journal of Geophysics and Engineering.* 2014(6), 063001. [CrossRef]
17. Stevens, S.H.; Kuuskraa, V.A.; Spector, D.; Riemer, P. CO_2 sequestration in deep coal seams: pilot results and worldwide potential. *Fuel and Energy Abstracts.* 2000.[CrossRef]
18. Pagnier, H.; Bergen, F.V.; Krzystolik, P.; Skiba, J.; Jura, B.; Hadro, J.; Wentink, P.; De-Smedt, G.; Kretzschmar, H.J.; Fröbel, J.; Müller-Syring, G.; Krooss, B.; Busch, A.; Wolf, K.H.; Mazumder, S.; Bossie-Codreanu, D.; Choi, X.; Grabowski, D.; Hurtevent, D.; Gale, J.; Winthaegen, P.; van der Meer, B.; Kobiela, Z.; Bruining, H.; Reeves, S.; Stevens, Scott. Field experiment of ECBM-CO_2 in the Upper Silesian Basin of Poland (RECOPOL). *Greenhouse Gas Control Technologies 7*. 2005, 1391-1397.[CrossRef]
19. Liu, Y.F.; LI, X.C.; Bai, B. Preliminary estimation of CO_2 storage capacity of coalbeds in China. *Chinese Journal of Rock Mechanics and Engineering.* 2005, 24(16), 2947-2952.[CrossRef]
20. Li, X.; Wei, N.; Liu, Y.; .CO_2 point emission and geological storage capacity in China.*Energy Procedia.* 2009, 1(1), 2793-2800.[CrossRef]
21. Ye, J.P.; Feng, S.L.; Fan, Z.Q.; Wang, G.Q; Gunter, W.D.; Wong, S.; Robinson, J.R. Micro-pilot test for enhanced coalbed methane recovery by injecting carbon dioxide in south part of Qinshui Basin. *Acta Petrolei Sinica.* 2007, 28(4), 77-80.[CrossRef]
22. François, C.; Placet, V.; Beaugrand, J.; Pourchet, S.; Boni, G.; Champion, D.; Fontaine, S.; Plasseraud, L. Can supercritical carbon dioxide be suitable for the green pretreatment of plant fibres dedicated to composite applications? *Journal of Materials Science.* 2020, 55(11), 4671–4684. [CrossRef]
23. Vishal, V.; Ranjith, P.G.; Pradhan, S.P.; Singh, T.N. Permeability of sub-critical carbon dioxide in naturally fractured Indian bituminous coal at a range of down-hole stress conditions. *Engineering Geology*. 2013,167,148–56. [CrossRef]
24. Patel, M.J.; May, E.F.; Johns, M.L. High-fidelity reservoir simulations of enhanced gas recovery with supercritical CO_2. *Energy*. 2016, 111:548–59. [CrossRef]
25. Simeoni, G. G.; Bryk, T.; Gorelli, F. A.; Krisch, M.; Ruocco, G.; Santoro, M.; Scopigno, T. The Widom line as the crossover between liquid-like and gas-like behaviour in supercritical fluids. *Nature Physics.* 2010, 6(7), 503–507. [CrossRef]
26. Adschiri, T. Supercritical Fluid Technology. *In The Expanding World of Chemical*

Engineering. 2019,105–123. [CrossRef]

27. Tomasko, D. L.; Guo, Z. Supercritical Fluids. In Kirk-Othmer Encyclopedia of Chemical Technology. *Wiley*. 2006.[CrossRef]
28. Calcara, M.; Caricaterra, M. CO_2 Dipole Moment: A Simple Model and Its Implications for CO2-Rock Interactions. *Minerals*. 2023, 13(1), 87. [CrossRef]
29. Di Maio, D. V.; Boccitto, A.; Caruso, G. Supercritical carbon dioxide applications: features and advantages. *2015 5th International Youth Conference on Energy* (IYCE). 2015,1–4. [CrossRef]
30. Marziale, A. 6. Synthesis in supercritical carbon dioxide. *In Supercritical Fluid Chromatography*. 2018, 127–162. De Gruyter. [CrossRef]
31. Liu, S.; Shi, R.; Yang, Y.; Li, L.; Wang, G. Effect of Supercritical Carbon Dioxide Treatment on Physical Properties of Polypropylene Films. *Journal of Applied Polymer Science*. 2024, 142(10). [CrossRef]
32. Sodeifian, G.; Usefi, M. M. B. Solubility, Extraction, and Nanoparticles Production in Supercritical Carbon Dioxide: A Mini-Review. *ChemBioEng Review*. 2022, 10(2), 133–166. [CrossRef]
33. Fu, C.Q.; Kou, X.; Du, Y.; Jiang, L.L.; Sang, S.X.; Pan, Z.J. Experimental study of supercritical CO_2-H_2O-coal interactions and the effect on coal spontaneous imbibition characteristics. *Fuel*. 2025, 383, 133888.[CrossRef]
34. Liu, C.; Wang, G.; Sang, S.; Rudolph,V. Changes in pore structure of anthracite coal associated with CO_2 sequestration process. *Fuel*. 2010, 89, 2665–72. [CrossRef]
35. Xu, S.C.; He, Z.X.; Long, R.Y.; Chen, H.; Han, H.M.; Zhang, W.W. Comparative analysis of the regional contributions to carbon emissions in China. *Journal of Cleaner Production*. 2016, 127, 406–417. [CrossRef]
36. Yang, J.; Guo, Q. Study on carbon emission estimation methods and emission reduction pathways at provincial level——Ningxia as an example. *Journal of Desert Research*. 2023, 43(05), 176-185. [CrossRef]
37. Qi, C.; Meng, J.; Che, B.; Kang, J.; Zhao, Y.; Hua, Z. Transition to a zero-carbon energy system in the Ningxia area: integrated CO_2 reduction measures from the multi-level perspective. *Frontiers in Energy Research*. 2023, 11. [CrossRef]
38. Liu, S.Q.; Mo, H.; Sang, S.H.; Liu, T. Source-sink matching and cluster deployment of carbon capture, utilization, andstorage in Ningxia Hui Autonomous Region. *Journal of China Coal Society*. 2024, 49(3), 1583−1596. [CrossRef]

39. Li, J.G.; He, W.; Zheng, Y. Sedimentary characteristics and coal accumulation law of Yan'an Formation coal seam in Yuanyanghu coal mine. *Clean Coal Technology*. 2014, 20(3), 57-65. [CrossRef]
40. Jiu, B.; Huang, W.; Sun, Q. Distribution Characteristics and Enrichment Model of Germanium in Coal: An Example from the Yimin Coalfield, Hailar Basin, China. *Natural Resources Research*. 2020, 30(1), 725–740. [CrossRef]
41. Senior, C.; Granite, E.; Linak, W.; Seames, W. Chemistry of Trace Inorganic Elements in Coal Combustion Systems: A Century of Discovery. *Energy & Fuels*. 2020, 34(12), 15141–15168. [CrossRef]
42. Dai, S.; Finkelman, R. B.; French, D.; Hower, J. C.; Graham, I. T.; Zhao, F. Modes of occurrence of elements in coal: A critical evaluation. *Earth-Science Reviews*. 2021, 222, 103815.[CrossRef]
43. Qin, S.J.; Lu, Q.F.; Li, Y.H; Wang, J.X.; Zhao, Q.J.; Gao, K. Relationships between trace elements and organic matter in coals. *Journal of Geochemical Exploration*. 2018, 188, 101−110.[CrossRef]
44. Finkelman, R. B.; Dai, S.; French, D. The importance of minerals in coal as the hosts of chemical elements: A review. *International Journal of Coal Geology*. 2019, 212, 103251.[CrossRef]
45. Jiu, B.; Huang, W.H.; Spiro, B.; Hao, R.L.; Mu, N.N.; Wen, L.; Hao, H.D. Distribution of Li, Ga, Nb, and REEs in coal as determined by LA-ICP-MSimaging: A case study from Jungar coalfield, Ordos Basin, China. *International Journal of Coal Geology*. 2023, 267, 104184.[CrossRef]
46. Kimura, T. Relationships between inorganic elements and minerals in coals from the Ashibetsu district, Ishikari coal field, Japan. *Fuel Processing Technology*. 1998, 56(1–2), 1–19.[CrossRef]
47. Li, B.; Jian, W.; Zhang, J.; Wang, B.; Zhu, D. Analysis of the Change Feature and Action Mechanism of Coal Pore Structure under the Action of Supercritical CO_2. *International Journal of Energy Research*. 2023, 1–13.[CrossRef]
48. Chen, R.; Zhang, Y.; Hu, K.; Tu, G.; Dou, T. Changes in Physicochemical Properties of Coal and Their Mechanism Due to Supercritical CO_2–H_2O Treatment. *Minerals*. 2023, 13(10), 1262. [CrossRef]
49. Zippa, E.; Zuddas, P.Estimation the reactive surface area of minerals during fluid-rock interaction in hydrothermal Jiangxi Province (SE China). *Applied Geochemistry*. 2020,

120, 104675.[CrossRef]

50. Zhang, K.; Sang, S.; Liu, C.; Ma, M.; Zhou, X. Experimental study the influences of geochemical reaction on coal structure during the CO_2 geological storage in deep coal seam. *Journal of Petroleum Science and Engineering.* 2019, 178, 1006–1017.[CrossRef]
51. Li, L.; Liu, X.; Nie, B.; Sun, H.; Jia, X.; Zhang, C. Microstructural alterations of coal induced by interaction with sequestered supercritical carbon dioxide. *Energy.* 2024, 304, 131912. [CrossRef]
52. Li, X.; Yu, H.; Lebedev, M.; Lu, M.; Yuan, Y.; Yang, Z.; Cheng, W.; Chen, S.; Zhan, J.; Ding, S.; Johnson, L.The Influence of CO_2 Saturated Brine on Microstructure of Coal: Implications for Carbon Geo-Sequestration. *Frontiers in Energy Research.* 2022, 10.[CrossRef]
53. Li, Z.; Xu, Y.; Yang, L.; Guo, J.; Chen, J. Physical and numerical simulations of the presence of a forsterite transitional zone at high temperature and pressure: insight for $scCO_2$ geological storage. *Australian Journal of Earth Sciences.* 2016, 63(4), 503–512.[CrossRef]
54. Presley, B. J. Trace Element Pollution. *In Water Encyclopedia.* 2004, 109 – 113. Wiley. [CrossRef]
55. Liu, X.; Zhang, C.L.; Nie, B.S; Zhang, C.P. Song, D.Z.; Yang, T.; Ma, Z.T. Mechanical response and mineral dissolution of anthracite induced by supercritical CO_2 saturation: Influence of saturation time. *Fuel.* 2022, 319, 123759. [CrossRef]
56. Sing, K.S.W. Reporting physisorption data for gas/solid systems with special reference to the determination of surface area and porosity (Recommendations 1984) . *Pure and Applied Chemistry.* 1985, 57(4), 603-619. [CrossRef]
57. Zhao, J.; Xu, H.; Tang, D.; Mathews, J.P.; Li, S.; Tao, S. A comparative evaluation of coal specific surface area by CO_2 and N_2 adsorption and its influence on CH_4 adsorption capacity at different pore sizes. *Fuel.* 2016,183,420 – 431.[CrossRef]
58. Hu, B.; Cheng, Y.; He, X.; Wang, Z.; Jiang, Z.; Wang, C.; Li, W.; Wang, L. New insights into the CH_4 adsorption capacity of coal based on microscopic pore properties. *Fuel.* 2020, 262, 116675.[CrossRef]
59. Marković, S.; Marković, Z.; McCrindle, R.; Simonović, B. Kinetics of extraction of coal-tar pitch components with supercritical carbon dioxide. *Chemical Papers.* 2007, 61(1).[CrossRef]
60. Zhang, D.; Gu, L.; Li, S.; Lian, P.; Tao, J. Interactions of Supercritical CO_2 with Coal.

Energy & Fuels. 2013, 27(1), 387 − 393.[CrossRef]

61. Li, R.; Wen, H.; Fan, S.; Wang, H.; Cheng, X.; Mi, W.; Liu, B.; Liu, M. Migration characteristics of constant elements in the process of coal dissolution by liquid CO_2. *Energy*. 2024, 295, 131006.[CrossRef]
62. Kolak, J.J.; Burruss, R.C. Geochemical investigation of the potential for mobilizing non-methane hydrocarbons during carbon dioxide storage in deep coal beds. *Energy & Fuels*. 2006, 20(2), 566-574.[CrossRef]
63. Du, Y., Sang, S., Wang, W., Liu, S., Wang, T., & Fang, H. (2018). Experimental Study of the Reactions of Supercritical CO_2 and Minerals in High-Rank Coal under Formation Conditions. *Energy & Fuels,* 32(2), 1115 − 1125. .[CrossRef]
64. Song, Y.; Zou, Q.L.; Su, E.L.; Zhang,Y.J.; Sun, Y.J. Changes in the microstructure of lowrank coal after supercritical CO_2 and water treatment. *Fuel*. 2020, 279, 118493.[CrossRef]